Enhancement of Char Gasification in CO_2 during Chemical Looping Combustion

Ewa J. Marek[*a], Yaoyao Zheng[a], Stuart. A. Scott[a]

[a]Department of Engineering, University of Cambridge, Trumpington Street, Cambridge, CB2 1PZ, United Kingdom

*Corresponding author, ejm94@cam.ac.uk

Abstract

Three chars were gasified in CO_2 in a fluidised bed of inert sand or Fe_2O_3 as an oxygen carrier (either derived from an ore or prepared in the laboratory). Rates of gasification were found to increase with temperature and the presence of active oxygen carriers. The observed change varied both with the chars' and carriers' reactivity. A numerical model was developed to simulate char gasification. It accounts for: intrinsic kinetics of gasification, intraparticle mass transfer in the char, external mass transfer in the particulate phase of the fluidised bed and CO combustion in the bed of Fe_2O_3. At 1223 K, CO was removed from the vicinity of the char on being oxidised by an oxygen carrier; this was accompanied by a simultaneous increase in CO_2 concentration, reducing the limitation imposed by mass transfer. It was concluded that the acceleration of gasification by oxygen carriers is significant only if gasification is limited by mass transfer in the first place. In addition, an analytical solution has been proposed, to combine all the processes into one simplified expression for estimating the apparent gasification rate. The influence of the intraparticle resistance was introduced with the effectiveness factor; the gasification rate was linearized with a Taylor series; finally the processes in the particulate phase were described with an enhancement factor, based on the Hatta number. This simple analytical model allows one to predict the influence of an oxygen carrier on the gasification of char during chemical looping combustion. The proposed expression for the effective rate was used to construct a map of the enhancement expected for various kinetic characteristics of an oxygen carrier.

Keywords: chemical looping combustion, CLC, gasification, kinetics, oxygen carrier

Nomenclature

A	Pre-exponential factor in Arrhenius expression for a rate constant (same units as its rate constant)
A_G	Coefficient in the linearized expression for gasification of char (s^{-1})
A_p	Particle surface (m^2)
B_G	Coefficient in the linearized expression for gasification of char (s^{-1})
c_{CO_2}, c_{CO}	Molar concentration of CO_2 and CO (mol m^{-3})

C_G	Coefficient in the linearized expression for gasification of char (mol m^{-3} s^{-1})
d_p	Particle diameter (m)
D_{AB}	Molecular diffusivity (m^2 s^{-1})
D_e	Effective diffusivity of a gas component (m^2 s^{-1})
E_a	Activation energy (kJ mol^{-1})
F	Enhancement factor (-)
$f(X_{char})$	Function of char conversion, representing relative change in the surface area (-)
$f(X_{OC})$	Function of conversion of oxygen carrier, representing relative change in the surface area (-)
$k_{g,CO}$, k_{g,CO_2}	Mass transfer coefficients (m s^{-1})
k_L	Mean mass transfer coefficient (m s^{-1})
k_i	Intrinsic rate constant of CO combustion with oxygen carrier (s^{-1})
$k_{Fe_2O_3}$	Apparent rate constant of CO combustion with oxygen carrier (s^{-1})
k_{-1}, k_1	Rate constants per active carbon centre (mol s^{-1} $bar^{-1)}$
k_2	Rate constants per active carbon centre (mol s^{-1})
$K_{p,char}$	Equilibrium constant for char gasification (-)
K_{p,Fe_2O_3}	Equilibrium constant for CO combustion on Fe_2O_3 (-)
M_C	Carbon molar weight (g mol^{-1})
N_{CO_2}, N_{CO}	Molar flux of CO_2 and CO (mol m^{-2} s^{-1})
p_{CO_2}, p_{CO}	Partial pressure of CO_2 and CO (bar)
r_g	Intrinsic rate of gasification (mol g^{-1} s^{-1})
$r'_{char,max}$	Maximum rate of gasification (mmol s^{-1} g^{-1})
r_p	Radius of char particle (m)
$r_{p,t}$	Radius of char particle at time t (m)
R	Universal gas constant (kJ mol^{-1} K^{-1})
R_G	Volumetric rate of gasification (mol s^{-1} m^{-3})
$R_G(X_{char})$	Gasification rate at conversion X_{char} (mol s^{-1} m^{-3})
$R_{G,eff}$	Effective rates of gasification (mol s^{-1} m^{-3})
R_p	Particle radius of oxygen carrier (m)
R_{OC}	Rate of CO combustion with oxygen carrier (mol s^{-1} m^{-3})
Sh	Sherwood number (-)
U_{mf}	Minimum superficial fluidising velocity (m s^{-1})

Greek letters

δ	Thickness of the mass transfer boundary layer (m)
γ	Hatta number (-)
ε_{char}	Char porosity
ε_{mf}	Voidage in the particulate phase (-)
ρ_{char}	Char molar density (mol m^{-3})
η	Radial position after coordinate transformation (-)

η_{char}	Effectiveness factor for gasification of char (-)
$\eta_{Fe_2O_3}$	Effectiveness factor for Fe_2O_3 reduction (-)
$\eta_{overall}$	Overall effectiveness of char gasification
v	Kinematic viscosity ($m^2\ s^{-1}$)
τ	Tortuosity (-)
Φ	Thiele modulus (-)

Subscripts

$bulk$	In the bulk
$char$	In regards to the gasification of char
Fe_2O_3	In regards to CO combustion with oxygen carrier
s	Particle surface

1. Introduction

Direct combustion of a solid fuel by contact with a solid oxygen carrier in chemical looping combustion (CLC) is improbable, at least with typical oxygen carriers, such as Fe_2O_3 [1]. In the classical form of chemical looping, conversion of the solid fuel to a gaseous form is required, and the gaseous product combusts in a reaction with an oxygen carrier. Alternatively, carriers, which release oxygen into the gas phase can be used, as in the CLOU process, allowing for a direct combustion of the solid fuel [2].

Conversion from a solid to a gaseous fuel can involve gasification by CO_2 or H_2O prior to combustion with an oxygen carrier or gasification carried out *in-situ* in the fuel reactor [3]. In both cases, if gasification takes place at moderate temperatures and low pressures, it is relatively slow, which will most likely limit the overall rate of CLC [4]. Besides the slow conversion of fuel, finding suitable oxygen carriers could also be problematic. Lyngfeld [4] suggested that the implementation of CLC with solid fuels at industrial scale will require inexpensive, naturally occurring minerals to be used as oxygen carriers. This is mostly due to the quick deactivation of the oxygen carrier in the presence of impurities carried by the solid fuel. A large makeup of material is needed, which is uneconomic unless cheap oxygen carriers can be found.

Finally, the effective performance of solid fuel gasification during CLC may not be easy to predict. The result depends not only on the fuel's properties and process parameters, as in the conventional combustion but also on the properties of the oxygen carrier. These, however, are rarely reported together, as a complementary set of attributes describing a CLC setup. Gasification, in the presence of an oxygen carrier, can be influenced by the combustion of a gaseous product, which makes the overall process challenging to assess. Previous studies report that an increase in the rate of char conversion was observed during the in-situ gasification in CLC [5]. Saucedo *et al.* [6] suggested that the acceleration of the observed rate is connected only to mass transfer, which often controls gasification. If a very reactive fuel is gasified in the diffusion-controlled-regime, the consumption of the gasification products by the oxygen carrier may reduce the mass transfer restriction. This was supported by the fact that the gasification

rate was not increased if the process was carried out at low temperatures, where it was instead limited by slow reaction kinetics.

So far, the main conclusion is that the enhancement depends on a set of conditions, at which gasification takes place. Process parameters, oxygen carrier's reactivity and kinetics of char gasification - all must be considered. This study analysed the problem comprehensively. First, the kinetics of char gasification in CO_2 and the kinetics of CO combustion with oxygen carrier were evaluated separately. Then, the gasification of char in CO_2 was carried out in the presence of oxygen carrier, as in chemical looping. Finally, for the combined situation: *in-situ* gasification of char and combustion of the gasification product using an oxygen carrier, we proposed a simplified model to quickly evaluate the effective rate of gasification.

2. Experimental

2.1. Fuels and bed materials

Three fuels were used in the gasification experiments: activated carbon, and two lignite chars: Polish char and a German char. The first one, a relatively unreactive activated carbon (Sigma-Aldrich C2889, peat bog char), was only crushed and sieved to 650-800 μm prior to the experiments. The last two fuels were prepared from Polish lignite coal (Belchatow area) and German Hambach lignite coal. Coals were pyrolysed in a fluidised bed (i.d. 78 mm) in a continuous flow of hot nitrogen at 1173 K for 2 h. Then the bed was cooled to room temperature, also in N_2. Resulting chars were sieved to 650-800 μm. The German char was prepared and described by Saucedo [7]. The proximate analysis for each char is given in Table 1.

Table 1. Proximate analysis of chars.

Parameter (wt%)	Polish char	German char	Activated carbon
Moisture	3.9	2.3	6.0
Ash	8.42	10.71	6.35
Volatiles	12.07	5.28	4.67
Fixed carbon	75.6	81.7	82.9

Three materials were fluidised as the bed material for experiments on gasification:

1. Silica sand (David Ball Group), 250-355 μm; washed twice in de-ionized water and dried for 24 h at 393 K. It was assumed throughout this study that SiO_2 was inert.
2. Roasted pyrite (Hessjøgruva AS, Norway), 100-250 μm; prepared from Norwegian pyrite ore by roasting in a fluidized bed (i.d. 78 mm) at 1023 K in the air (0.5×10^{-3} m^3 s^{-1}). This allowed for iron sulphide converting into iron oxide according to: $2FeS_2 + 5.5O_2 \rightarrow Fe_2O_3 + 4SO_2$. Roasting was performed in a bed of limestone (850-1000 μm, (Longcliffe Quarries Ltd), to capture SO_2. Separation of the roasted pyrite from the bed was carried out firstly with sieves, then with a magnet. The resulting material contained

~ 90 wt% Fe_2O_3, estimated using a temperature programmed reduction performed in H_2 in a TGA. XRF results showed trace amounts of Cu, Ca and Zn in the roasted material.

3. Iron oxide particles, 100-250 µm; prepared from powder (Sigma Aldrich) by mechanical mixing with 2 wt% PVA water solution; calcined in air at 1273 K for 3 h and sieved. As shown later in Fig. 4, Section 4: Results, the resulting particles were initially unreactive and needed activating; without activation, gasification in Fe_2O_3 was very similar to the experiments with inert SiO_2. The activation was performed in a fluidized bed by a long reduction in a $CO/CO_2/N_2$ mixture (3.7 vol% CO, 25 vol% CO_2, rest N_2), followed by re-oxidation in an $O_2/CO_2/N_2$ mixture (5 vol% O_2, 15 vol% CO_2, rest N_2). Both reduction and oxidation were carried out until gas composition at the outlet did not change and the concentrations were identical to those at the inlet. This procedure resulted in an increase in the reactivity (Fig. 5).

2.2. Experimental setup

Most experiments were performed in the fluidized bed, illustrated in Fig. 1. The bed was held in a quartz reactor, with a porous disk (grade 1) as the distributor, located 110 mm from the gas inlet. The reactor was heated electrically by a tubular furnace (up to 1223 K). From the top of the reactor, a K-type thermocouple was inserted for controlling the temperature, by measuring the temperature of the bed material ~ 1 cm above the porous disk. Gas flows, provided to the bottom of reactor, were controlled with a system of solenoid valves and rotameters. Outlet gas was sampled with a pump (16 mL s^{-1}) and passed through a drying tube (filled with $CaCl_2$), then directed to an NDIR analyser (ABB EL3020) to measure the concentrations of CO and CO_2.

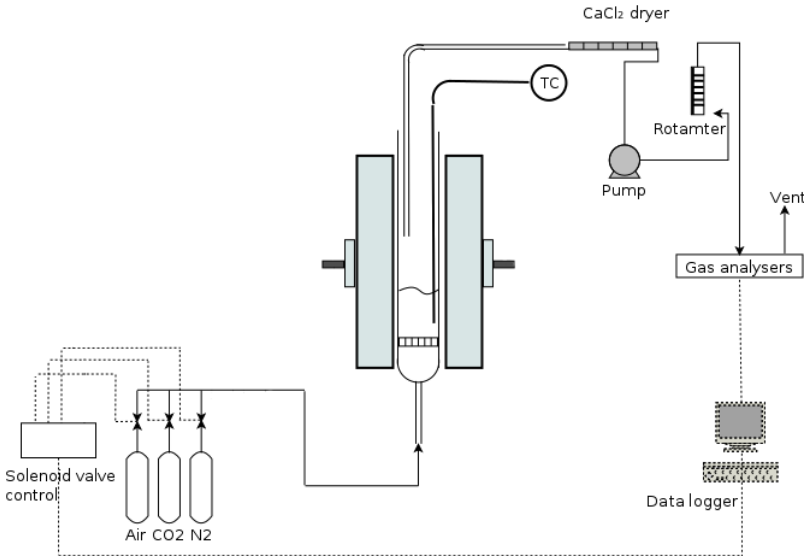

Fig. 1. Experimental setup with small-scale fluidised bed (i.d. 25 mm). TC represents a thermocouple.

2.3. Char gasification experiments

Gasification experiments were performed by dropping a batch of fuel (0.1 g) to the fluidized bed, made of silica sand or one of the active materials (15 cm^3, unfluidised). A mixture of 20 vol% CO_2/N_2, used as the gasifing agent, was provided to the bottom of the reactor

(40 mL s^{-1}, NTP), resulting in U/U_{mf} ~ 12 (U_{mf} evaluated with Wen and Yu's correlation [8]). Experiments were performed at 5 temperatures, from 1123 to 1223 K in steps of 25 K.

Gasification was carried out until no CO was measured at the outlet, typically for 5 to 240 min., depending on the temperature, fuel and bed material used. After each experiment, the reactor was purged with nitrogen and then air was introduced for 5 min., in order to re-oxidize the active material.

2.4. Kinetics of char gasification

Gasification in CO_2 was firstly investigated in SiO_2, an inert material. Kinetic parameters for the gasification of the German lignite char were taken from the study by Saucedo *et al* [7]. For the Polish char and activated carbon a set of gasification experiments was performed in SiO_2 (15 cm^3, unfluidized), with a small batch of fuel (~0.04 g) being dropped into the fluidised bed. Experiments were performed between 1123 K and 1223 K, in steps of 25 K, using CO_2/N_2 mixtures, where CO_2 concentration was varied between 20 and 100 vol%. Exemplary results for the gasification in 20 vol% CO_2/N_2 are presented in Fig. 5.

The overall reaction for gasifying a solid fuel with CO_2 is:

$$C_s + CO_{2(g)} \leftrightarrow 2CO_g \tag{1}$$

The two-step mechanism for char gasification proposed by Ergun [9] assumes:

1. On adsorption, a molecule of CO_2 leaves a chemisorbed atom of oxygen and gaseous CO:

$$C^* + CO_{2(g)} \overset{k_1/k_{-1}}{\longleftrightarrow} C(O) + CO_{(g)} \tag{2}$$

The reverse reaction involves the detachment of the adsorbed atom of oxygen by a CO molecule, forming CO_2 in the gas phase.

2. The C(O) complex can detach from the char, yielding CO into the gas phase, with possibly the creation of new active carbon sites (n = 0, 1 or 2):

$$C(O) \overset{k_2}{\rightarrow} nC^* + CO_{(g)} \tag{3}$$

For a heterogeneous set of reactions involving sorption-desorption processes, a Langmuir-Hinshelwood expression for the overall rate of char conversion, r_g(mol g^{-1} s^{-1}) emerges:

$$r_g = \frac{ck_2\left(p_{CO_2} - \frac{p_{CO}^2}{K_{p,char}}\right)}{p_{CO_2} + (k_2/k_1) + (k_{-1}/k_1)p_{CO}} \tag{4}$$

where c is the concentration of active centres in a unit mass of fuel; k_{-1}, k_1, k_2 are the rate constants per active carbon centre; p_{CO_2}, p_{CO} represent partial pressures of CO_2 and CO; $K_{p,char}$ is the equilibrium constant for Reaction (1). For the equilibrium constant in Reaction (2) the following relation was proposed [9]:

$$k_{-1}/k_1 = 2.4 \times 10^{-4} \exp\left(-E_{a_{k_{-1}/k_1}}/RT\right) \tag{5}$$

with the activation energy, E_a = -95 kJ mol^{-1}, independent of the type of char.

Expression (4) for the rate of char gasification was first introduced by Ergun [9] and later the term $p_{CO}^2/K_{p,char}$ in the nominator was added to allow for reversibility of

reaction (1) [10,11]. This term, however, is usually negligible (at low temperatures p_{CO} is close to 0, while at higher temperatures K_p increases quickly; in both cases $p_{CO}^2/K_{p,char} \to 0$).

As gasification progresses, the char's properties change. To account for the evolution of the available surface area, the char reaction rate R_G (mol s^{-1} m^{-3}), as proposed by Dai *et al.* [11], can be related to the experimentally measured function of char conversion $f(X_{char})$, *i.e.*

$$R_G = r_g \rho_{char} f(X_{char}) M_C \quad (6)$$

with ρ_{char} being the char's molar density, M_C is the molar weight of carbon and $f(X_{char})$ is the conversion function, determined as $f(X_{char}) = R_G(X_{char})/R_{G,X_{char}=0.01}$ and obtained experimentally at a temperature at which particles react uniformly across the cross-section (kinetic regime). Here, $f(X_{char})$ was obtained by fitting a polynomial (septic) function to the gasification results at 1123 K. $R_G(X_{char})$ and $R_{G,X_{char}=0.01}$ are gasification rates at conversions X_{char} and the initial conversion, chosen to be X_{char} = 0.01.

Rearranging Ergun's expression (4) and ignoring p_{CO}^2/K_p term in the nominator gives a linear relation between the initial gasification rate, $r_{g,0}$ and the constants, ck_1 and ck_2:

$$\frac{p_{co_2}}{r_{g,0}} = \frac{1}{ck_2}\left(p_{CO_2} + \frac{k_{-1}}{k_1} p_{CO}\right) + \frac{1}{ck_1} \quad (7)$$

By applying the Arrhenius' law for ck_1 and ck_2 it is possible to evaluate activation energies and pre-exponential coefficients for both kinetic constants. Here, the kinetic parameters were experimentally determined for the Polish char and for activated carbon. The Arrhenius plots obtained are presented in the Supplementary Information (SFig. 1). The set of all the kinetic constants is given in Table 2.

Table 2: Kinetic parameters for the rate constants of char gasification, as expressed with Ergun's equation. Values for the German lignite char were taken from [7].

Fuel	A_{ck1}, (mol s^{-1} g^{-1} bar^{-1})	E_{ck1}, (kJ mol^{-1})	A_{ck2}, (mol s^{-1} g^{-1})	E_{ck2}, (kJ mol^{-1})
Polish char	2.46×10^6	237	1.61×10^{11}	162
German char	2.56×10^6	200	1.26×10^{11}	290
Activated carbon	2.10×10^6	216	2.25×10^{11}	273

2.5. Kinetics of the reduction of active materials

Reduction of oxygen carrier was characterised separately from the gasification of chars, using CO from a cylinder (in mixture with CO_2 and N_2). For reduction of Fe_2O_3 with CO:

$$3Fe_2O_{3(s)} + CO_{(g)} \rightarrow 2Fe_3O_{4(s)} + CO_{2(g)} \quad (8)$$

$$1.200Fe_3O_{4(s)} + CO_{(g)} \rightarrow 3.801Fe_{0.947}O_{(s)} + CO_{2(g)} \quad (9)$$

During an *in-situ* char gasification in CO_2, a high concentration of CO_2 is expected in the bulk gas, to keep the rate of char conversion high. Due to the presence of CO_2, the reduction

of Fe_2O_3 will be limited and the main reaction occurring will be the reduction of hematite to magnetite (R. 8). The same assumption will be valid in industrial CLC systems [1].

In order to evaluate the kinetics of Fe_2O_3 reduction, redox cycling experiments, analogous to the one in [12] were performed. A typical experiment started with a blank cycle (no sample in the reactor), then a sample of the oxygen carrier (0.02-0.05 g) was dropped into the fluidised bed, where it was subjected to 8 redox cycles. A single cycle consisted of a reduction and an oxidation step. Reduction of the carrier was done in a mixture of 3.7 vol% CO, 25 vol% CO_2 and N_2 for 5-15 min. Oxidation of the carrier lasted for 5 min. and was carried out in a mixture of 5 vol% O_2, 15 vol% CO_2 and N_2. In between, the bed was flushed with N_2 for 1 min. By keeping a high CO_2/CO ratio (6.76) it was possible to prevent reduction of iron oxide to wustite or metallic iron. Experiments were carried out at 723-973 K. The duration of the reduction and the gas flowrates were adjusted with temperature to allow for the complete transition of hematite to magnetite and to keep $U/U_{mf} \sim 9$. Exemplary profiles of CO and CO_2 measured in the experiments are presented in the Supplementary Information (SFig. 2).

Assuming a first order reaction, the rate of CO combustion by reacting with oxygen carrier in R. (8), R_{OC} (mol s^{-1} m^{-3}), is:

$$R_{OC} = \mathrm{k_i c_{CO}} = Aexp\left(-\frac{E_a}{RT}\right)\left(c_{CO} - \frac{c_{CO2}}{K_{p,Fe2O3}}\right) f(X_{OC}) \quad (10)$$

with A and E_a being kinetic parameters, $K_{p,Fe2O3}$ is the equilibrium constant for reaction (8). $f(X_{OC})$ represents the function of the particle's conversion. In the experiments, where a batch of char was gasified in the presence of oxygen carrier, the amount of metal oxide was in excess (Section 2.3). Thus, the conversion of oxygen carrier was negligible and can be assumed to be $X_{OC} = 0$; i.e. $f(X_{OC}) \sim 1$ simplifying eq. (10).

To account for diffusional effects, the experimentally determined rate constant, $k_{Fe_2O_3}$, was analysed using the total resistance method, as described by Bohn [13]:

$$\frac{1}{k_{Fe_2O_3}} = \frac{R_p}{3k_{g,CO}} + \frac{1}{\eta_{Fe2O3} k_i} + \frac{R_p}{k_{g,CO2} K_{p,Fe2O3}} \quad (11)$$

where $k_{Fe_2O_3}$ is the apparent rate coefficient, R_p is the radius of a particle of oxygen carrier, $k_{g,CO}$ and k_{g,CO_2} are mass transfer coefficients, k_i is the intrinsic rate constant, respectively $\eta_{Fe_2O_3} = \frac{3}{\phi^2_{Fe_2O_3}}(\phi_{Fe2O3} coth\phi_{Fe2O3} - 1)$ is the effectiveness factor for Fe_2O_3 reduction, with $\phi_{Fe2O3} = R_p\sqrt{\frac{k_i}{D_{e,CO}} + \frac{k_i}{D_{e,CO_2}}}$. The effective diffusivity of the gas component is given as $D_e = \frac{\varepsilon_{p_{Fe2O3}} D_{AB}}{\tau^2_{Fe2O3}}$, where $\varepsilon_{p_{Fe2O3}}$ represents the porosity of the particle, τ_{Fe2O3} its tortuosity and D_{AB} molecular diffusivity. For both active materials the fitted values of $\varepsilon_{p_{Fe2O3}} = 0.5$ and $\tau_{Fe2O3} = 2.5$ were used.

Calculations for k_i were carried out iteratively, using as the first approximation of k_i the value obtained from the experimental results and assuming effectiveness factor $\eta_{Fe2O3} = 1$. The iterations were carried out until η_{Fe2O3} converged to a stable value. The mass transfer

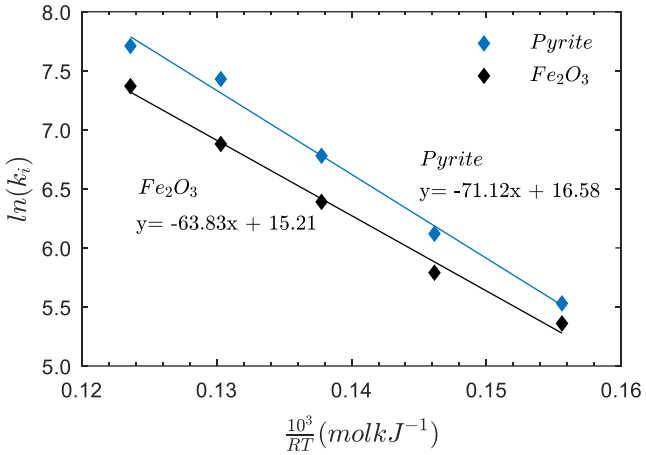

Fig. 2. Arrhenius plots for the reduction of oxygen carriers: roasted pyrite and synthesized Fe_2O_3. Results obtained from initial reduction rates, $r'_{Fe_2O_3}$, of hematite to magnetite reduction carried in: 3.7 vol% CO, 25 vol% CO_2 and N_2.

coefficients, $k_{g,CO}$ and $k_{g,CO2}$, were calculated using $k_g = (2R_pSh)/D_{AB}$, where Sherwood number was obtained with eq. (21). The ratio between the experimental $k_{Fe_2O_3}$ and the converged value of k_i indicates the importance of mass transfer and the range of implemented correction. For both materials, $k_{Fe_2O_3}/k_i$ decreased with temperature, from 0.97 at 723 K to 0.77 at 973 K. At the highest temperature, the correction was imposed by the resistance from intraparticle diffusion ($\eta_{Fe_2O_3}$~85%).

Finally, the kinetic parameters were evaluated assuming the Arrhenius equation for the rate constant: $k_i = Aexp(-E_a/(RT))$. Fig. 2 shows the Arrhenius plots obtained for both oxygen carriers. For pyrite the activation energy was found to be 71 kJ mol^{-1} with corresponding pre-exponential factor A = 1.6×10^7 s^{-1}. For iron oxide particles the values are E_a = 64 kJ mol^{-1} and A = 0.42×10^7 s^{-1}. The obtained parameters are in good agreement with the values reported in the literature [14,15] for Fe_2O_3 particles.

After characterising the gasification of chars in CO_2 and reduction of oxygen carriers with CO separately, the experiments of char gasification in CO_2 in the presence of an oxygen carrier were conducted. The results are presented in Section 4.

3. Models

3.1. Approximate analytical solution

The 1-D model used here describes the gasification of a single char particle when surrounded by oxygen carrier particle. Solid fuels in the presence of CO_2 or H_2O are converted to combustible gaseous products through the gasification reactions (R. 2 and 3). For (2) to occur, the gasifying agent (CO_2) needs to diffuse towards the char particle from the bulk. Similarly, the product of the reactions (R. 2 and 3), CO is transferred in the opposite direction, away from the char. At moderate temperatures, as investigated here, char gasification is slow (see Fig. 4). This makes the transient change in CO and CO_2 concentrations negligible and allows one to assume pseudo-steady-state conditions. Moreover, to keep the analysis simple, a

dilute flow and pseudo-binary mixture were also assumed, allowing Fickian fluxes to be used. With the above simplifications, a component balance over a differential volume in the gas phase was expressed as:

$$0 = \frac{D_{e,g}}{r^2}\frac{\partial}{\partial r}\left(r^2\frac{\partial c}{\partial r}\right) \quad (12)$$

where $D_{e,g} = D_{AB} \cdot \varepsilon_{mf}$ is the effective diffusivity through the gas layer, affected by the particular matter (bed material) and ε_{mf} is the voidage in the particulate phase.

When gasification takes place in a CLC system, the balance within the differential volume should also consider the reaction involving oxygen carrier. Thus, eq. (12) becomes:

$$0 = \frac{D_{e,gCO_2}}{r^2}\frac{\partial}{\partial r}\left(r^2\frac{\partial c_{CO_2}}{\partial r}\right) + \eta_{Fe2O3}k_i \cdot c_{CO} \quad (13)$$

$$0 = \frac{D_{e,gCO}}{r^2}\frac{\partial}{\partial r}\left(r^2\frac{\partial c_{CO}}{\partial r}\right) - \eta_{Fe2O3}k_i \cdot c_{CO} \quad (14)$$

Since the gasification experiments were carried out at high temperatures, some influence of mass transfer within a particle of the oxygen carrier can be expected. To account for that, R_{OC}, the rate of CO combustion was multiplied by the effectiveness factor for Fe_2O_3 reduction, $\eta_{Fe_2O_3}$ (described in sec. 3.5). Equations 13 and 14 can be summed up, leading to:

$$0 = \frac{D_{e,gCO_2}}{r^2}\frac{\partial}{\partial r}\left(r^2\frac{\partial c_{CO_2}}{\partial r}\right) + \frac{D_{e,gCO}}{r^2}\frac{\partial}{\partial r}\left(r^2\frac{\partial c_{CO}}{\partial r}\right) \quad (15)$$

By applying boundary conditions:

$$c_{CO_2} = c_{CO_2,bulk}, c_{CO} = c_{CO,bulk} = 0 \; at \; r \rightarrow \mathrm{r_p} + \delta \quad (16)$$

$$c_{CO_2} = c_{CO_2,s}, c_{CO} = c_{CO,s} \; at \; r \rightarrow \mathrm{r_p} \quad (17)$$

equation (14) can be solved independently as:

$$\mathrm{c_{CO}} = \frac{\mathrm{r_p}}{\mathrm{r}}\mathrm{c}_{CO,s}\frac{\sinh\left((\gamma\left(1-\frac{r-r_p}{\delta}\right)\right)}{\sinh(\gamma)} \quad (18)$$

where r_p is the radius of the char particle, γ is the Hatta number: $\gamma = \delta\sqrt{\eta_{\mathrm{Fe2O3}}\mathrm{k_i}/D_{e,gCO}}$, and δ is the thickness of gas boundary layer around the char particle. The value of δ was calculated using Hayhurst's expression [16], together with the Sherwood number for equimolar counter-diffusion (EMCD) [17]. The result was corrected for fluidized bed experiments in a reactor of a small diameter [18], by multiplying by a correction factor α:

$$Sh_{EMCD} = 2\varepsilon_{mf}(1 + r_p/\delta) \quad (19)$$

$$\mathrm{Sh_{EMCD}} = \alpha\,(2\varepsilon_{\mathrm{mf}} + 0.69\left(\frac{2r_pU_{mf}}{v\epsilon_{\mathrm{mf}}}\right)^{\frac{1}{2}}\left(\frac{v}{D_{AB,CO2}}\right)^{\frac{1}{3}}) \quad (20)$$

where ν is the kinematic viscosity. As r_p is the particle radius, then the distance from particle centre to the bulk is $\mathrm{r}_\infty = r_p + \delta$. The correction factor, $\alpha = 2$, was experimentally determined by Mao [18] and accounts for the differences in experimentally determined Sherwood number, as measured for fluidisation in a reactor of very small diameter, similar to the one used here. The Sherwood number was assumed constant throughout the char conversion.

The concentration of CO_2 was obtained by solving eq. (15):

$$c_{CO_2} = \frac{r_p}{r}\frac{(2r_p+\delta-r)}{r_p+\delta}\left(\frac{D_{e,gCO}}{D_{e,gCO_2}}c_{CO,s} + c_{CO_2,s} - c_{CO_2,bulk}\right) + c_{CO_2,bulk} - \frac{D_{e,gCO}}{D_{e,gCO_2}}c_{CO} \quad (21)$$

Using the above solution for CO (eq. 18), the CO flux from the particle surface can be calculated:

$$N_{CO}|_{r=r_p} = -D_{e,gCO}\frac{\partial c_{CO}}{\partial r} \tag{22}$$

With the pseudo-steady state assumption (no accumulation), the CO_2 flux is linked to the CO flux:

$$N_{CO_2}\Big|_{r=r_p} = -\frac{1}{2}N_{CO}\Big|_{r=r_p} \tag{23}$$

As CO diffuses away from the char particle, it is being consumed by the oxygen carrier. This is analogous to the mass transport and reaction through a liquid layer, which is often described using an enhancement factor. It is assumed that the gas layer around the char particle is stagnant and is responsible for all of the mass transfer resistance, meaning when there is no reaction the rate of CO transfer from the char-gas interface (particle surface) to the bulk is:

$$N_{CO}|_{r=r_p}\mathrm{A_p} = k_{g_{CO}}\left(c_{CO,s} - c_{CO,bulk}\right)A_p = k_{g_{CO}}c_{CO,s}A_p \tag{24}$$

where $\mathrm{A_p}$ is the particle surface and the mass transfer coefficients for the CO transport in the gas is: $k_{g_{CO}} = D_{e,gCO}(\delta + r_p)/(\delta r_p)$.

The simultaneous and, as assumed here, irreversible chemical reaction with the oxygen carrier consumes CO and increases the mass transfer rate. The overall result can be assessed with an enhancement factor, F_{CO}, defined as:

$$F_{CO} = \frac{N_{CO}}{k_{g_{CO}}(c_{CO,s} - c_{CO,bulk})} = \frac{N_{CO}}{k_{g_{CO}}c_{CO,s}} \tag{25}$$

where N_{CO} is the actual flux, enhanced by the chemical reaction and $k_{g_{CO}}\left(c_{CO,s} - c_{CO,bulk}\right)$ represents the mass transfer resistance if there was no reaction. Moreover, it can be connected to the CO flux at the particle surface, eq. (22):

$$F_{CO} = \frac{D_{e,gCO}\left(\delta + \gamma r_p\, coth(\gamma)\right)}{\delta k_{g_{CO}} r_p} \tag{26}$$

This result differs from that commonly found in the literature, because it was derived for spherical coordinates, with the important assumption of $c_{CO,bulk} = 0\ at\ r \to \mathrm{r_p} + \delta$. If there is no reaction in the gas phase, then γ=0, F_{CO}=1 and the rate of mass transfer is that for diffusion only.

As CO is consumed, CO_2 is created, and the rate of mass transfer of CO_2 is also enhanced, however, in the opposite direction. For the pseudo-steady-state, eq. (23) also applies when there is an enhancement of the external mass transfer. That implies that the enhancement factor needs to be the same both for CO and CO_2:

$$F_{CO_2} = F_{CO} = F \tag{27}$$

Finally, the connection between processes inside the char particle and its surrounding comes through the fluxes on the surface, where the steady-state assumption imposes that the total amount for each component entering/leaving needs to be equal to the generation/consumption of the component in the particle:

$$F k_{g,CO_2}\left(c_{CO_2,s} - c_{CO_2,bulk}\right) = -\eta_{char}R_G\,\frac{r_p}{3} \tag{28}$$

$$Fk_{g,CO}\, c_{CO,s} = 2\eta_{char} R_G \frac{r_p}{3} \tag{29}$$

Here, the intraparticle mass transfer is introduced through the effectiveness factor, η_{char} and the external mass transfer is described with the enhancement factor, F and the Hatta number, γ.

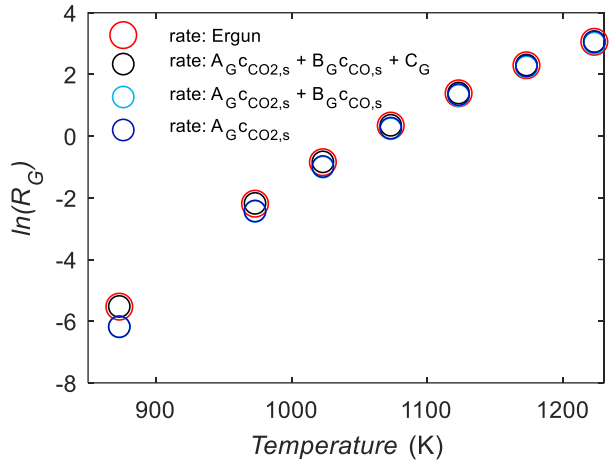

Fig. 3. Comparison of gasification rates calculated for German lignite char using full Ergun expression, or simplified linearized forms. Rates were calculated for maximum values of $f(X)$. Above 1073 K all simplified rates are within 5% error in respect to the rate obtained using full Ergun's expression.

To simplify the analysis, the rate of gasification can be linearized. If a Taylor series centred on the species concentrations in the bulk is applied on the Ergun's expression, then the rate of char gasification (eq. 4) becomes:

$$\mathrm{R_G} = \mathrm{A_G c_{CO_2,s}} + \mathrm{B_G c_{CO,s}} + \mathrm{C_G} \tag{30}$$

where A_G, B_G and C_G are the linearization coefficients:

$$A_G = (ck_2)\frac{1}{RT}\frac{k_2}{k_1}\rho_{0,char} f(X) M_c / \left(\frac{1}{RT}\frac{k_2}{k_1} + c_{CO_2,bulk}\right)^2 \tag{31}$$

$$B_G = -c_{CO_2,bulk}(ck_2)\frac{k_{-1}}{k_1}\rho_{0,char} f(X) M_c / \left(\frac{1}{RT}\frac{k_2}{k_1} + c_{CO_2,bulk}\right)^2 \tag{32}$$

$$C_G = c^2_{CO_2,bulk}(ck_2)\rho_{0,char} f(X) M_c / \left(\frac{1}{RT}\frac{k_2}{k_1} + c_{CO_2,bulk}\right)^2 \tag{33}$$

A_G, B_G and C_G change with temperature and conversion, and represent char properties through the kinetic constants, $k_1, k_2, \frac{\mathrm{k_{-1}}}{\mathrm{k_1}}$, and the conversion function f(X).

Despite the simplification, the linearized expression gives rates very close to those from the full Ergun's equation. In fact, the linearized expression can be simplified further by dropping the term C_G or both $B_G c_{CO} + C_G$, and effectively changing the equation into an irreversible, first-order reaction rate expression. The error introduced with such simplification depends on temperature and char characteristics, mostly its sensitivity to CO inhibition. For the fuels in this study, the rates estimated for the activated carbon and the Polish lignite were found only up to 1.6% different than the rates calculated with the full Ergun's equation, for T = 873-1223 K. In case of the German lignite char, as presented in Fig. 3, the rate in the form $R_G = A_G c_{CO_2}$ was about 50% of the value evaluated with the full rate at T = 873K. The discrepancy quickly diminished with temperature, and the error less than 5% was noted at T > 1073 K.

Solving eq. (28) and (29) for $c_{CO_2,s}$ and $c_{CO,s}$and using the linearized rate $R_G = A_G c_{CO_2} + B_G c_{CO} + C_G$, then gives an analytical expression for effective rate of char gasification in the presence of the oxygen carrier, $R_{G,eff}$:

$$R_{G,eff} = \frac{3F\eta_{char}k_L(C_G + A_G c_{CO,2,bulk})}{3Fk_L + A_G\eta_{char}r_p - 2B_G\eta_{char}r_p} \quad (34)$$

where k_L is the mean mass transfer coefficient.

The proposed overall rate, $R_{G,eff}$, gathers information about gasification conditions (T, $c_{CO_2,bulk}$), fuel reactivity and its conversion function (present in the A_G, B_G and C_G coefficients), intraparticle mass transfer (η_{char}), and external mass transfer (k_{L,CO_2}), including the influence from the reaction with the oxygen carrier (F).

To evaluate the effectiveness factor for char gasification η_{char}, needed in eq. (28) and (29), the approach presented in [19] was applied. For a Langmuir-Hinshelwood type of reaction, the rate can alternatively be expressed as:

$$R_g = \frac{k' p_{CO_2,s}}{1 + K_{CO}p_{CO,s} + K_{CO_2}p_{CO_2,s}} \quad (35)$$

where k' is the modified rate constant, while K connects the parameters for all species present in the system:

$$k' = ck_1\rho_{char} \cdot f(X_{char})/\omega \quad (36)$$

$$K_{CO} = k_{-1}/k_2 \quad (37)$$

$$K_{CO_2} = k_1/k_2 \quad (38)$$

Sundaram [20] then gives the effectiveness factor in terms of:

$$K = \frac{K_{CO_2} - \frac{D_{e,p2}}{D_{e,p1}} \cdot K_{CO} v_{CO}}{\omega} \quad (39)$$

$$\omega = 1 + \frac{D_{e,p2}}{D_{e,p1}} p_{CO_2,s} v_{CO} + K_{CO} p_{CO,s} \quad (40)$$

Here, $v_{CO} = 2$ is the stoichiometric coefficient for CO in the gasification reaction. The effective diffusivity of gas component transported through the char matrix $D_{e,p}$ can be calculated with its molecular diffusivity D_{AB} after [6] as $D_{e,p} = D_{AB}\left(\varepsilon_{char,0} + \left(1 - \varepsilon_{char,0}\right)X_{char}(t)\right)/{\tau_{char}}^2$, where $\varepsilon_{char,0}$ is the initial char porosity, $X_{char}(t)$ represents the char conversion and τ_{char} is the particle tortuosity (assumed here to be 2).

A modified Thiele modulus was also evaluated [19]:

$$\Phi = \frac{r_p}{3}\left(\frac{k'RT}{D_{e,pCO_2}}\right)^{0.5} \quad (41)$$

The effectiveness factor, η_{char}, for the Langmuir-Hinshelwood rate equation was evaluated numerically by Sundaram [20] and can be calculated as:

$$\eta_{char} = tanh(f\Phi^*)/\Phi^* \quad (42)$$

where $\Phi^* = \frac{\Phi}{\Phi_C}$, $\Phi_C = \sqrt{2}\frac{\left(1 + Kp_{CO_2,s}\right)}{Kp_{CO_2,s}}\left(Kp_{CO_2,s} - \ln\left(1 + Kp_{CO_2,s}\right)\right)^{0.5}$ and $f = 1 - 0.4457\left(Kp_{CO_2,s}\right)^2\Phi^*\exp\left(-0.1153\Phi^*\right)$.

To evaluate η_{char} concentration of both species on the particle surface are needed. These can be obtained by solving again for fluxes on the particle surface, using c_{CO_2} eq. (18) and c_{CO} from eq. (21):

$$-D_{e,gCO_2}\frac{\partial c_{CO_2}}{\partial r} = -\eta_{char}R_G\,\frac{r_p}{3} \tag{43}$$

$$-D_{e,gCO}\frac{\partial c_{CO}}{\partial r} = 2\eta_{char}R_G\frac{r_p}{3} \tag{44}$$

Because eq. (43 and 44) depend on the reaction rate, then by introducing further eq. (4 or 30), a set of coupled equations for $c_{CO_{2,s}}$ and $c_{CO,s}$ is obtained. This needs to be solved simultaneously, as species concentrations on the surface depend on η_{char}. A similar approach has been used previously, using full Ergun's rate [6]. The closed solution for $c_{CO_{2,s}}$ and $c_{CO,s}$, obtained here for the linearized rate, is presented in the Supplementary Document.

3.2. Numerical solution

Because the analytical approach was simplified (assumed steady-state conditions, no particle radius change, an average conversion for the whole char particle), a numerical approach was also proposed. This time no steady-state conditions were assumed, hence a component balance (for CO_2 or CO) over a differential volume of the char particle was:

$$\frac{\partial c\varepsilon_{char}}{\partial t} = \frac{D_{e,p}}{r^2}\frac{\partial}{\partial r}\left(r^2\frac{\partial c}{\partial r}\right) + xR_G \tag{45}$$

where ε_{char} is the char porosity, r is the radial position in the particle, x is a stoichiometric coefficient in respect to gasification reaction ($x = -1$ for CO_2, $x = 2$ for CO) and R_G is the rate of gasification calculated with eq. (6).

For the case in which diffusional effects are dominant, the reaction occurs primarily in a thin outer layer, resulting in a change of radius (r_p) with time. To model the transition between fully kinetic control, i.e. no gradients in conversion and falling density, to the strong diffusional control, in which the particle shrinks ($r_p(t) = r_{p,t}$), a coordinate transformation is needed and was implemented here by setting $\eta = \frac{r}{r_{p,t}}$, which fixes the solid/gas interface at $\eta = 1$. Same approach was applied previously in char combustion, when reaction is mostly limited to the surface [21,22]. The new coordinate system introduces a pseudo-convective term in all time-derivative equations, thus for the component balance inside the particle ($0 < \eta \leq 1$) eq. (45) becomes:

$$\frac{\partial c\varepsilon_{char}}{\partial t} = \frac{D_{e,p}}{r_{p,t}^2\eta^2}\frac{\partial}{\partial \eta}\left(\eta^2\frac{dc}{d\eta}\right) + xR_G + \frac{\eta}{r_{p,t}}\frac{\partial c}{\partial \eta}\frac{dr_p}{dt} \tag{46}$$

where the derivative $\frac{dr_p}{dt}$ refers to a moving boundary velocity, that was calculated with the rate of change of particle density at the most outer layer ($r = r_p$) [22]:

$$\frac{dr_p}{dt} = \frac{\left(\frac{d\rho}{dt}\right)_{r=r_{p,t}}}{\left(\frac{d\rho}{dr}\right)_{r=r_{p,t}}} = \frac{R_{G_{\eta=1}}}{\left(\frac{1}{r_{p,t}}\frac{d\rho}{d\eta}\right)_{\eta=1}} \tag{47}$$

The material balance in the solid particle gives the density change at fixed $\eta \leq 1$ as:

$$\frac{\partial \rho}{\partial t} = -xR_G - \frac{\eta}{r_{p,t}} \frac{\partial \rho_{char}}{\partial \eta} \frac{dr_p}{dt} \quad (48)$$

The component balance over a differential volume of the gas phase around the particle ($1 < \eta \leq \frac{r_\infty}{r_{p,t}}$) was represented as:

$$\frac{\partial c \varepsilon_{mf}}{\partial t} = \frac{D_{e,g}}{r_{p,t}^2 \eta^2} \frac{\partial}{\partial \eta} \left(\eta^2 \frac{\partial c}{\partial \eta} \right) - \frac{\eta}{r_{p,t}} \frac{\partial c}{\partial \eta} \frac{dr_p}{dt} \quad \text{for } SiO_2 \text{ as bed material (49)}$$

$$\frac{\partial c \varepsilon_{mf}}{\partial t} = \frac{D_{e,g}}{r_{p,t}^2 \eta^2} \frac{\partial}{\partial \eta} \left(\eta^2 \frac{\partial c}{\partial \eta} \right) - z\eta_{Fe2O3} R_{OC} - \frac{\eta}{r_{p,t}} \frac{\partial c}{\partial \eta} \frac{dr_p}{dt} \quad \text{for active bed material(50)}$$

with z being a stoichiometric coefficient for a component in the CO combustion with an oxygen carrier ($z = -1$ for CO_2, $z = 1$ for CO). Again, the last term in eq. (49 and 50) accounts for the moving interface.

Calculations for CO and CO_2 molar concentrations were carried out by applying boundary conditions:

$$c_{CO} = 0 \; at \; \eta \rightarrow \frac{r_\infty}{r_{p,t}} \quad (51)$$

$$c_{CO_2} = c_{CO_2,bulk} \; at \; \eta \rightarrow \frac{r_\infty}{r_{p,t}} \quad (52)$$

$$\frac{dc}{dr} = 0 \; at \; \eta = 0 \quad (53)$$

and initial conditions at t = 0:

$$c_{CO}(\eta, \, \mathrm{t} = 0) = 0 \text{ for } 0 < \eta < \frac{r_\infty}{r_{p,t}} \quad (54)$$

$$c_{CO_2}(\eta, \, \mathrm{t} = 0) = 0 \text{ for } 0 < \eta < 1 \quad (55)$$

$$c_{CO_2}(\eta, \, \mathrm{t} = 0) = c_{CO_2 \, bulk} \text{ for } 1 \leq \eta < \frac{r_\infty}{r_{p,t}} \quad (56)$$

In all simulations, the particle was treated as isothermal. The differential equations were discretised spatially, on a computational grid both within the particle and its gaseous surrounding. The equations were coded and solved by marching forward in time, in Matlab, using the ODE15s solver.

4. Results

Gas composition at the outlet of the fluidised bed was measured during the gasification experiments; Fig. 4 gives an example of the obtained profiles. In silica sand, the appearance of CO and the decrease in CO_2 concentration showed the progress of the gasification. In the active bed materials, the CO created in gasification was combusted, leading to an increase in CO_2 concentration above the values observed in SiO_2 bed. It is also worth noticing that in case of the roasted pyrite almost a complete combustion of CO was observed.

Fig. 5 presents rates of gasification for chars and bed materials, both obtained in experiments and simulated with the theoretical models. Experiments in SiO_2 showed that the reactivity of the fuels was of order: activated carbon < Polish lignite < German lignite.

When the bed material was switched from SiO_2 to the active one, a significant increase in the gasification rate was observed for both lignite chars at 1223 K. From two lignite chars at 1223 K, when active materials were introduced, the gasification rate of the German char increased more than for the Polish char. At the lower temperature, 1123 K, the effect was similar although much less pronounced. For the activated carbon, regardless of the temperature and bed material, the observed rates were almost the same.

Gasification in roasted pyrite was always faster than in Fe_2O_3 particles, providing that the influence from active materials was noticeable. The ore-derived material had lower nominal content of iron oxide than the synthesised Fe_2O_3 particles, which suggests that impurities from the natural mineral might have influenced the material characteristics. As it was described in Sec. 2.1 particles prepared from Fe_2O_3 powder were almost inactive immediately after calcination. The possible activation of the synthesised Fe_2O_3 particles, through a full redox cycle, indicates that the material properties also depend strongly on its structure and porosity.

Fig. 5 presents also the results of the simulations carried out with the simplified analytical approach (sec. 3.1) and with the numerical model (sec. 3.2). Gasification rates calculated

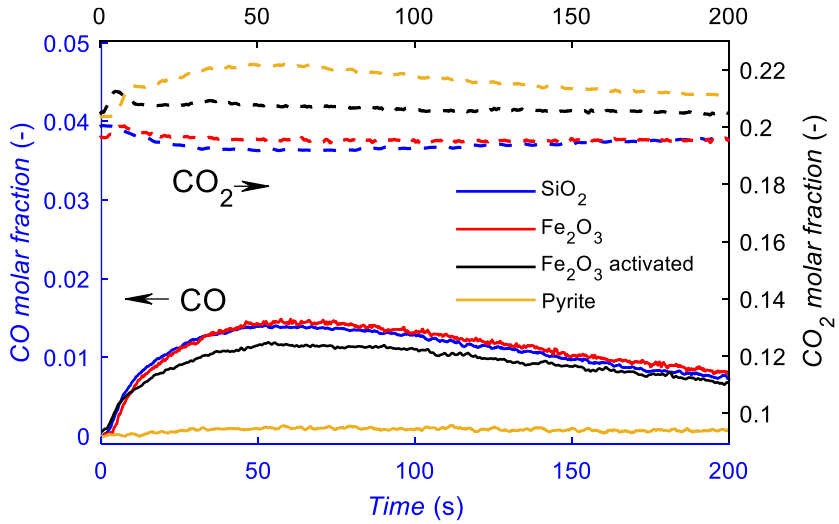

Fig. 4. CO and CO_2 profiles measured during the gasification experiments in inactive (SiO_2, fresh Fe_2O_3 particles) and active (activated Fe_2O_3, roasted pyrite) bed materials. The graph presents the results obtained for the German lignite char at T=1148 K.

numerically are in agreement with rates obtained in experiments. Thus, the kinetic parameters taken for the German lignite char from [7] and parameters determined here for the other two fuels seem to describe the gasification correctly, at all temperatures. The experimentally determined conversion function, $f(X)$, aimed to simulate the evolution of pore structure as char is being consumed. Indeed, its presence helped with modelling the shapes of rate curves correctly. This contrasts with Dai *et al.* [11], who gasified Hambach lignite char, produced from the same coal as the German char used in this study. They found the $f(X)$ function failed to predict the experimental results at higher temperatures. Despite that, the good agreement showed here and the simplicity of the $f(X)$ still make this approach very attractive in comparison to other, numerical models used for prediction of structure evolution.

Despite the fact that the calculated and experimental results agree, some discrepancies were noticed. In most cases, this can be investigated by checking if the assumptions behind the theoretical models were met, as will be discussed in section 5. Another possibility is that at low rates of reaction, i.e. at the lowest temperatures, the measured gas concentrations fall close to the detection limit. As a result, the experimental profiles might be underestimated.

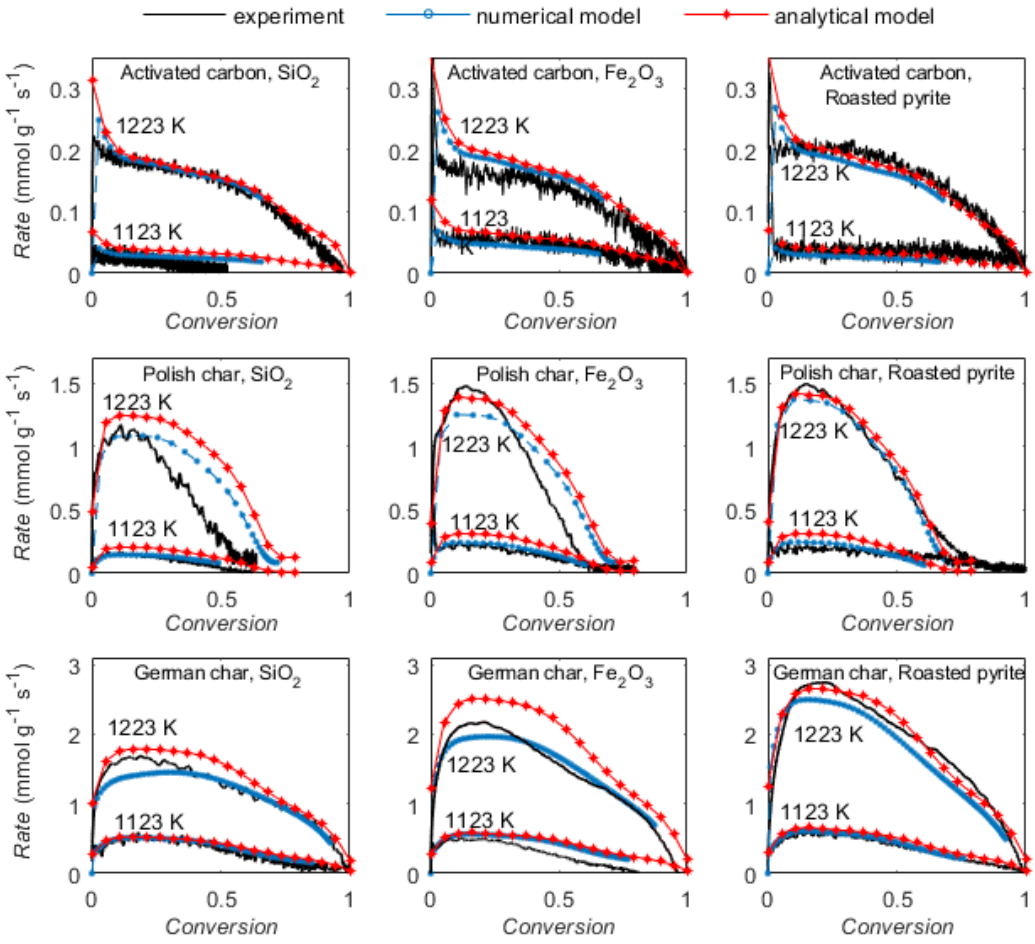

Fig. 5. Rates of char gasification from experiments (black) and simulated with the numerical model (blue) and simplified analytical model with linearised rate equation (red). Gasification carried out in SiO_2, Fe_2O_3 and roasted pyrite, at 1123 K and 1223 K (1148 K and 1223 K for the activated carbon in Fe_2O_3 particles due to a very low measurement signal at the lowest temperature).

5. Discussion

At high temperatures, gasification is often limited by the rate of diffusion of gaseous components. If gasification was controlled solely by the mass transfer, then the obtained rate would have been close to the theoretical maximum rate that can be observed [17]:

$$r'_{char,max} = 2 \times 0.91 \times Sh_{EMCD} D_{CO_2} c_{CO_2,bulk} \frac{6}{\rho_{char} d_p^2} \quad (57)$$

where d_p is the particle diameter and 0.91 corrects Sh_{EMCD} for a non-equimolar diffusion. At 1223 K, using parameters as in this study, the value of $r'_{char,max}$ would be 11 (mmol s^{-1} g^{-1}). This sets a reference value to the rates presented in Fig. 5. It is worth noticing that the gasification rate for the activated carbon was an order of magnitude lower than $r'_{char,max}$, suggesting that the conversion was limited by the reaction kinetics in all experiments. For two lignite chars, at the highest tested temperature, the obtained rates were significantly higher, indicating an increasing importance of the mass transfer.

Previous studies showed that the presence of an oxygen carrier enhances char gasification [6] at high temperatures if the mass transfer limitation is noticeable. At lower temperatures, the rate of gasification was not affected significantly, suggesting that in the kinetics limited regime, any consumption of the gasification products by the oxygen carrier does not influence the overall rate. Here, in case of activated carbon, no influence from oxygen carriers was observed in a broader range of studied temperatures because of the very low reactivity of the fuel that limited the overall rate of its gasification to the kinetic reaction rate. Moreover, as discussed before, chars kinetics indicate different sensitivity to the CO inhibition. This suggests that the removal of CO by the oxygen carrier may result in a different range of the rate enhancement for different chars.

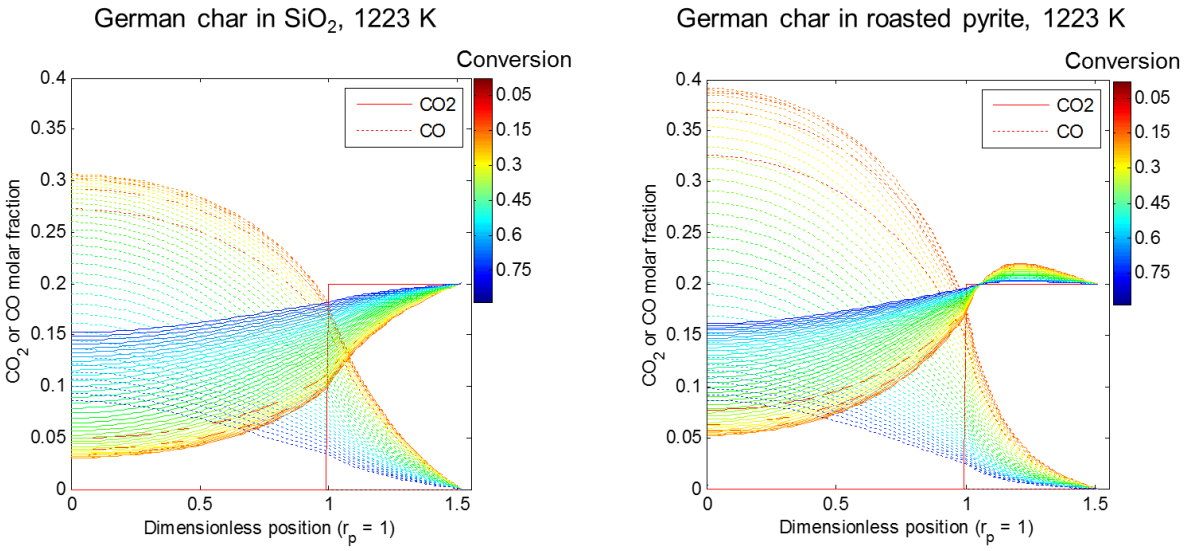

Fig. 6. Predicted CO and CO_2 concentrations during char gasification (German lignite) at 1223 K in a) SiO_2 and b) roasted pyrite. Dimensionless position ≤ 1 refers to the char particle, while > 1 to the surrounding. Change of line colour indicates char conversion and can be understood as a dimensionless duration of the gasification. Concentration profiles were calculated with the numerical model.

The simplest way to assess how diffusion limits the gasification rate is to analyse concentration gradients across particle. As shown in Fig. 6, for the gasification in SiO_2 of the German lignite char (1223 K), the accumulation of CO in the particle was continuously increasing and the gradient of CO_2 concentration was significant and spread from the bulk to the particle centre. For the gasification in the bed of active material, the gas profiles changed. As expected, CO was consumed in particle surrounding and its concentration in that region dropped. The reaction with the oxygen carrier led to CO_2 accumulation close to the particle surface and the resulting increase in the CO_2 level exceeded the value in the bulk. Both the change of CO and CO_2 concentration in the gas phase resulted in the increase of the overall gasification rate, which explains the experimental observations. Interestingly, the level of CO in the particle towards the end of the process was even higher than for the gasification in SiO_2; but so was the average concertation of CO_2. The later has more impact on the Ergun's rate, therefore the inhibition from the CO was masked.

The aim of the simplified rate expression, derived with the analytical model, was to present a way of rate evaluation, independent on the conditions in the surface, yet, inclusive to other process conditions. As presented in Fig. 5, the results were generally in agreement with rates obtained experimentally and through the numerical simulation. Nevertheless, it needs to be highlighted that the analytical approach required a few essential assumptions and simplifications. Besides the steady state conditions and no particle radius change, an average conversion for the whole char particle was assumed. This will be correct only if particle reacts uniformly and the diffusion of CO and CO_2 through the particle matrix is fast. This assumption is only strictly valid if there are no concentration gradients in the particle. In the simplified model, it was imposed by an average value of the $f(X)$ function. Moreover, for the external mass transfer, it was assumed that $c_{CO,bulk} = 0$, at the distance of δ (from the surface). This

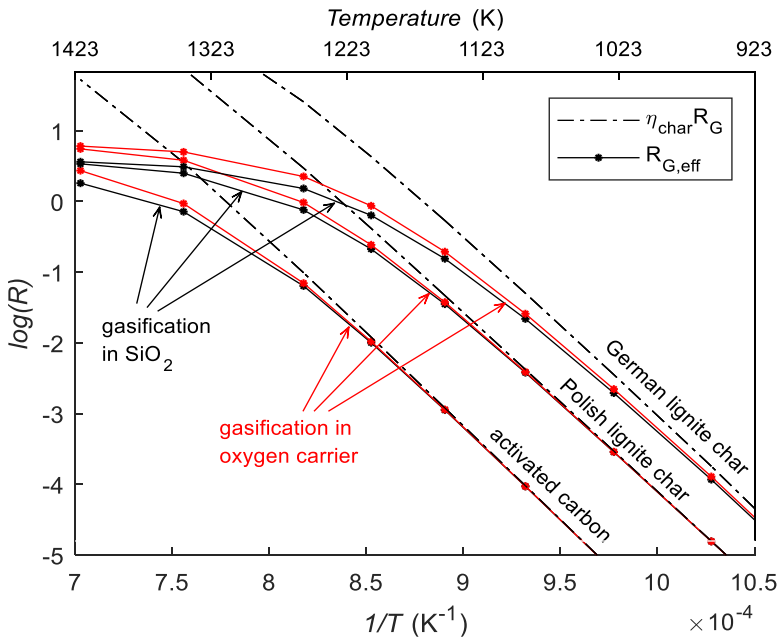

Fig. 7. Arrhenius plot for rates of gasification: influenced by intraparticle mass transfer only (dotted lines), influenced by intraparticle and external mass transfer (solid lines). Gasification carried out in SiO_2 or oxygen carrier (results for Fe_2O_3 and roasted pyrite overlap).

will hold only if the reaction in the film (gas phase + carrier particles) was fast, and $\gamma > 3$ [23]. In other cases, such as gasification in SiO_2, the analysis should account for the value of $c_{CO,bulk}$, (as included in eq. (59) and in the Supplementary Information). With that in mind, it is worth emphasizing that the results obtained with the effective rate expression were, nevertheless, reasonable in the whole temperature range.

Since the effective rate expression, $R_{G,eff}$, combines parameters of phenomena in the chemical looping setup, it can conveniently be used to analyse the influence of each of them. The importance of the changes in the external mass transfer can be investigated with the Arrhenius plots, as presented in Fig. 7. For the activated carbon, gasification was not restricted by the external diffusion up to 1223 K. With a further increase in the temperature, the rate started to deviate from the case calculated with no mass transfer resistance. This was not elevated by the presence of the oxygen carrier until an even higher temperature was reached, > 1300 K. For more reactive German lignite char, the influence from the external mass transfer was noticeable even at 923 K. At this conditions, CO combustion with Fe_2O_3-containing materials was slow due to the slow reaction kinetics. When the reaction rate increased, so did the influence from the oxygen carrier and the effective rate of char conversion significantly increased. Interestingly, as seen for the Polish lignite char, there seems to be a regime, in which the mass transfer limitation is present, yet the reaction with the oxygen carrier does not enhance the gasification. This is not due to slow Fe_2O_3 reduction, as the oxygen carrier enhances the gasification of the German char at the same conditions. On the other hand, there will be a transition period, when both external mass transfer and the reaction kinetics play similarly important roles.

Fig. 7 allows evaluating what is the starting temperature when the presence of oxygen carrier will accelerate the gasification rate. For both tested oxygen carriers, the influence on the rate is very similar. On contrary, it is the reactivity of the fuel that primarily influences the effective rate. To follow with these conclusions, a much broader range of char-oxygen carrier pairs will be needed, including oxides of metals other than Fe.

Eq. (34) can be directly non-dimensionalised to:

$$\frac{R_{G,eff}}{(C_G + A_G c_{CO,2,bulk})} = \frac{R_{G,eff}}{R_{G\,@\,bulk\ concentrations}} = \frac{1}{\frac{1}{\eta_{char}} + \frac{(A_G - 2B_G) r_p}{3 F k_g}} = \eta_{overall} \tag{58}$$

which compares the ratio of the effective rate to the maximum possible rate if the entirety of the char is gasified at bulk conditions (i.e. when the rate is $C_G + A_G c_{CO,2,bulk} + B_G c_{CO,bulk}$, with $c_{CO,bulk} = 0$) . The dimensionalised equation still holds if CO was present in the bulk:

$$\frac{R_{G,eff}}{(C_G + B_G c_{CO,bulk} + A_G c_{CO,2,bulk})} = \frac{1}{\frac{1}{\eta_{char}} + \frac{(A_G - 2B_G) r_p}{3 F k_g}} = \eta_{overall} \tag{59}$$

Here, however, the change in the CO bulk concentration needs to be also acknowledged in the derivation of the enhancement factor, F. The solution for F that applies, in this case, is provided in the Supplementary Information.

The right-hand side of the non-dimensional rate represents resistance in series:

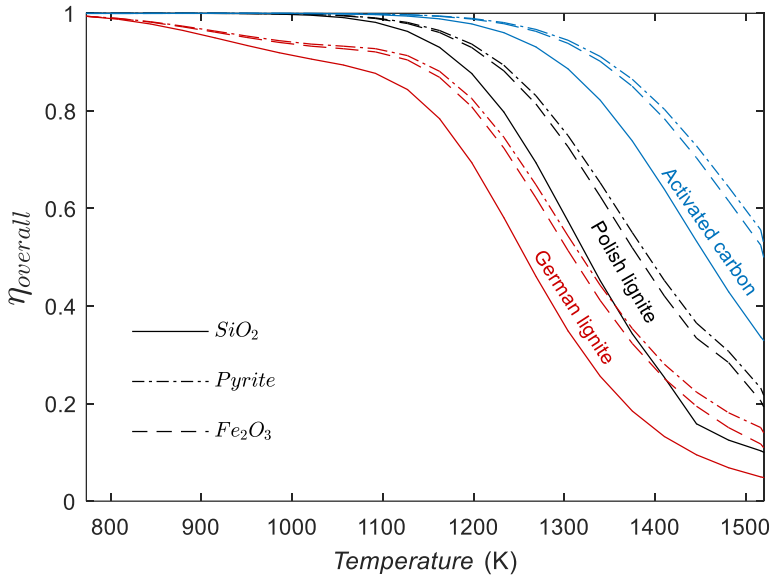

Fig. 8. Overall effectiveness for a comparison of the gasification rate to the maximum rate at bulk conditions. Calculated for the mean rates, across full char conversion. Gasification in SiO_2 or the oxygen carrier.

$$\frac{1}{k_o} = \frac{1}{\eta_{char}(A_G - 2B_G)} + \frac{1}{\frac{3}{r_p}Fk_L} \tag{60}$$

where k_o is the "overall" reaction coefficient. At low temperatures, when the effectiveness of gasification is high, the dominating term that limits the rate is $(A_G - 2B_G)$ from the reaction kinetics. Obviously, when the temperature is increased, the reaction accelerates, and the rate is limited by the mass transfer. In case of reaction with an oxygen carrier, F is >1, therefore the last term, describing the external mass transfer, $\frac{1}{\frac{3}{r_p}Fk_L}$, decreases. As a result, the influence from the mass transfer decreases. Additionally, the presence of the oxygen carrier influences η_{char}, that is calculated using surface concentrations. This, however, happens when the reaction in the char particle is almost instantaneous, therefore $\frac{1}{\eta_{char}(A_G - 2B_G)}$ still goes to 0.

Getting back to eq. (58), the comparison of the actual rate to the maximum possible rate gives a measure of an "overall" effectiveness of gasification, $\eta_{overall}$. It combines both intraparticle and external resistance and has a limit of ~1 when mass transport is fast. It is not possible to reach $\eta_{overall} = 1$, unless the last term, $\frac{(A_G - 2B_G)r_p}{3Fk_g}$, goes to 0. As B_G is always positive (see eq. 32), this happens only when there is no reaction with the char (A_G, B_G=0). Otherwise, the effect from the mass transport will be present, although in the kinetic regime, only very subtly. With temperature, both kinetic parameters, $(A_G - 2B_G)$, and mass transfer coefficient, k_L increase, and the ratio between them defines how quickly the influence from the external mass transport starts to be clearly noticeable.

Fig. 8 presents $\eta_{overall}$ for gasification in inert or active bed materials. For all three fuels the enhancement from the presence of oxygen carrier looks similar but shifted with the

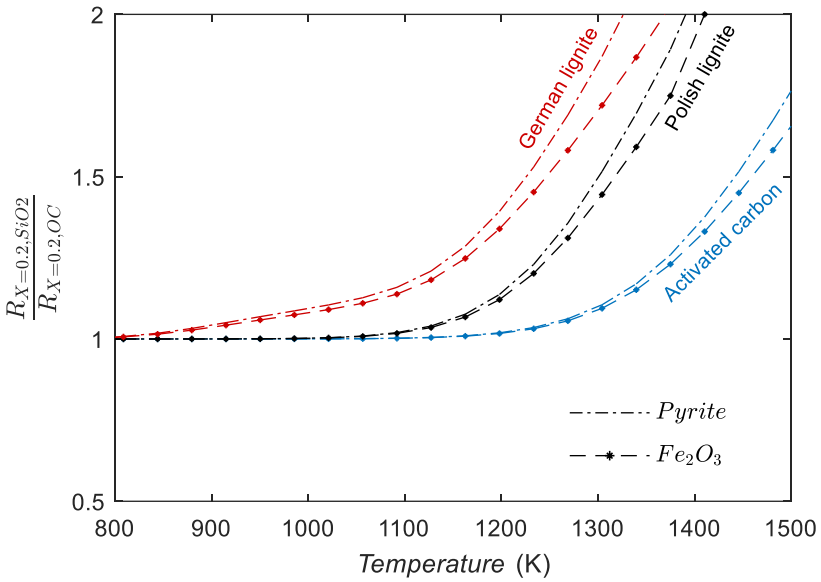

Fig. 9. Ratios of gasification rate in oxygen carrier to the gasification rate in SiO_2. Analysis performed for rates at char conversion, X = 0.2 (representing maximum rate).

temperature. The only noticeable difference can be seen for the German lignite char, where at lower temperatures it is sensitive to the presence of CO. At higher temperatures, the enhancement effect increases, which can also be seen in Fig. 9, where the rate in the presence of oxygen carrier is divided by the rate in SiO_2. In that reference, the enhanced rate is significantly higher, indicating the actual importance of the enhancement effect.

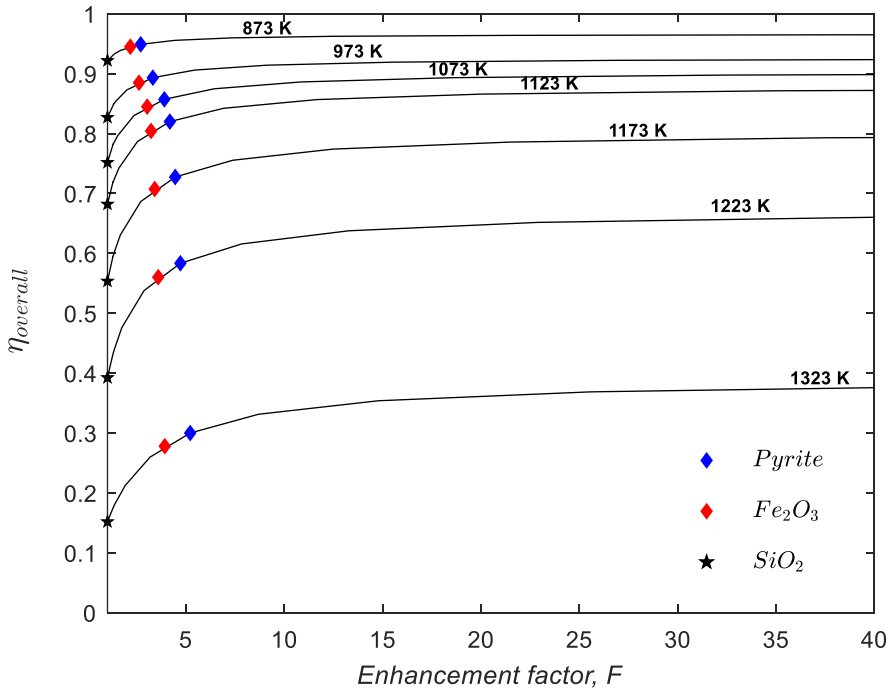

Fig. 10. Isothermal regions of possible rate enhancement. The analysis was carried out for German lignite char; rates were evaluated at char conversion X = 0.2 (representing maximum rate).

Finally, Fig. 10 gives the isothermal regions, that map values of the enhancement factor, F, and the overall effectiveness, $\eta_{overall}$, which arise when kinetic parameters of the oxygen carrier are varied. For SiO_2, i.e. k_i = 0 and F = 1, only internal and external mass transfer cause deviations from overall effectiveness = 1. Then, increasing k_i, i.e. making the material active, quickly increases the observed rate of gasification. Despite the slow kinetics of the reaction of the oxygen carrier, the enhancement is significant even at low k_i, because $\eta_{Fe_2O_3}$is close to one. When the kinetic coefficient k_i is higher, the enhancement effect is more pronounced as $\eta_{Fe_2O_3}$ falls. Nevertheless, there is a limit of the actual enhancement that results from the presence of the active material. For a "perfect" oxygen carrier, that is able to react with CO instantaneously, F increases to infinity. With that, the $(A_G - 2B_G)r_p/3Fk_L$ term in eq. (58) diminishes, and the "overall" effectiveness is no longer affected by the external mass transfer. Despite that, the resistance in the intraparticle diffusion stays mostly unaffected, therefore η_{char} limits the final value of the observed rate.

Here, we have presented an analysis of possible enhancement in the char gasification rate. The dependence of the rate on external mass transfer was first observed experimentally and later explained with the effective rate expression and the "overall" effectiveness. The main aim was to propose an operative approach, applicable for a quantitative evaluation of the "enhancement effect". By constructing isothermal maps, that are applicable to a specific char, it is possible to evaluate what enhancement can be expected if the fuel was gasified in chemical looping conditions. This approach does not apply in situations when oxygen carrier releases gaseous oxygen, however, a similar approach could be used to analyse the effect in a CLOU setup.

6. Conclusions

Gasification of char in CO_2 in the presence of oxygen carriers was investigated. For gasification governed by mass transfer, the presence of oxygen carriers increased the gasification rate significantly. On the contrary, when the process was governed by the kinetics, no significant change in the rate was observed on adding an oxygen carrier. Gasification rates were predicted accurately with a numerical model and a simplified analytical model. With the latter, a new expression for the effective rate of char gasification was proposed:

$$R_{G,eff} = \frac{3F\eta_{char}k_L(C_G + A_G c_{CO,2,bulk})}{3Fk_L + A_G\eta_{char}r_p - 2B_G\eta_{char}r_p}.$$

Despite its simple form, the effective rate combined influences from all the important phenomena: gasification kinetics, oxygen carrier's reactivity, intraparticle mass transfer in both char and the carrier, the external mass transfer and process conditions. The effective rate provides a new way for a simple, yet accurate prediction of the rate of gasifying a char with chemical looping. As an example, a map of the expected enhancements from the presence of oxygen carriers was presented and discussed.

Acknowledgments

This research was funded by EPSRC (project references: EP/L022427/1 and EP/K030132/1). Authors express gratitude to Dr Yngve Larring and Dr Mehdi Pishahang from Sintef, Norway for providing pyrite ore, Dr Ewelia Ksepko from IChPW, Poland for lignite char and Dr Marco Saucedo for preparing lignite char, Prof. Allan Hayhurst for helpful discussions.

Data

A set of all collected experimental and supporting data for this work can be found on https://www.repository.cam.ac.uk.

References

[1] J. Adanez, A. Abad, F. Garcia-Labiano, P. Gayan, L.F. de Diego, Progress in Chemical-Looping Combustion and Reforming technologies, Prog. Energy Combust. Sci. 38 (2012) 215–282. doi:10.1016/j.pecs.2011.09.001.

[2] T. Mattisson, Materials for Chemical-Looping with Oxygen Uncoupling, Int. Sch. Res. Not. 2013 (2013) e526375. doi:10.1155/2013/526375.

[3] A. Lyngfelt, Chemical-looping combustion of solid fuels – Status of development, Appl. Energy. 113 (2014) 1869–1873. doi:10.1016/j.apenergy.2013.05.043.

[4] A. Lyngfelt, T. Mattisson, M. Rydén, C.J. Linderholm, Chemical-Looping Combustion of Solid Fuels – What is needed to reach full-scale?, in: 4th Int. Conf. Chem. Looping Sept. 26-28 Nanjing China, 2016. https://research.chalmers.se/publication/250297 (accessed March 29, 2018).

[5] H. Leion, T. Mattisson, A. Lyngfelt, Solid fuels in chemical-looping combustion, Int. J. Greenh. Gas Control. 2 (2008) 180–193. doi:10.1016/S1750-5836(07)00117-X.

[6] M.A. Saucedo, J.S. Dennis, S.A. Scott, Modelling rates of gasification of a char particle in chemical looping combustion, Proc. Combust. Inst. 35 (2015) 2785–2792. doi:10.1016/j.proci.2014.07.005.

[7] M.A. Saucedo, J.Y. Lim, J.S. Dennis, S.A. Scott, CO_2-gasification of a lignite coal in the presence of an iron-based oxygen carrier for chemical-looping combustion, Fuel. 127 (2014) 186–201. doi:10.1016/j.fuel.2013.07.045.

[8] C.Y. Wen, Y.H. Yu, A generalized method for predicting the minimum fluidization velocity, AIChE J. 12 (1966) 610–612. doi:10.1002/aic.690120343.

[9] S. Ergun, Kinetics of the reaction of carbon with carbon dioxide, J. Phys. Chem. 60 (1956) 480–485.

[10] F. Scala, Fluidized Bed Technologies for Near-Zero Emission Combustion and Gasification, Elsevier, 2013.

[11] P. Dai, J.S. Dennis, S.A. Scott, Using an experimentally-determined model of the evolution of pore structure for the gasification of chars by CO_2, Fuel. 171 (2016) 29–43. doi:10.1016/j.fuel.2015.12.041.

[12] C.D. Bohn, J.P. Cleeton, C.M. Miiller, S.A. Scotr, J.S. Dennis, Measuring the Kinetics of the Reduction of Iron Oxide with Carbon Monoxide in a Fluidized Bed, in: G. Yue, H. Zhang, C. Zhao, Z. Luo (Eds.), Proc. 20th Int. Conf. Fluid. Bed Combust., Springer Berlin Heidelberg, 2009: pp. 555–561. doi:10.1007/978-3-642-02682-9_84.

[13] C.D. Bohn, The Production of Pure Hydrogen with Simultaneous Capture of Carbon Dioxide, Ph.D, thesis, University of Cambridge, 2010.

[14] C.D. Bohn, J.P. Cleeton, C.R. Müller, J.F. Davidson, A.N. Hayhurst, S.A. Scott, J.S. Dennis, The kinetics of the reduction of iron oxide by carbon monoxide mixed with carbon dioxide, AIChE J. 56 (2010) 1016–1029. doi:10.1002/aic.12084.
[15] Z. Zhang, T.P. Hills, S.A. Scott, P.S. Fennell, Spouted bed reactor for kinetic measurements of reduction of Fe_2O_3 in a CO_2/CO atmosphere Part I: Atmospheric pressure measurements and equipment commissioning, Chem. Eng. Res. Des. 114 (2016) 307–320. doi:10.1016/j.cherd.2016.06.028.
[16] A.N. Hayhurst, The mass transfer coefficient for oxygen reacting with a carbon particle in a fluidized or packed bed, Combust. Flame. 121 (2000) 679–688. doi:10.1016/S0010-2180(99)00178-9.
[17] A.N. Hayhurst, M.S. Parmar, Measurement of the mass transfer coefficient and Sherwood number for carbon spheres burning in a bubbling fluidized bed, Combust. Flame. 130 (2002) 361–375. doi:10.1016/S0010-2180(02)00387-5.
[18] R. Mao, The Investigation of Aspects of Chemical Looping Combustion in Fluidised Beds, Thesis, University of Cambridge, 2018. doi:10.17863/CAM.21679.
[19] G.W. Roberts, C.N. Satterfield, Effectiveness Factor for Porous Catalysts. Langmuir-Hinshelwood Kinetic Expressions, Ind. Eng. Chem. Fundam. 4 (1965) 288–293. doi:10.1021/i160015a009.
[20] K.M. Sundaram, Catalyst Effectiveness Factor for Langmuir-Hinshelwood-Hougen-Watson Kinetic Expressions, Chem. Eng. Commun. 15 (1982) 305–311. doi:10.1080/00986448208911076.
[21] G.R. Gavalas, Analysis of Char Combustion Including the Effect of Pore Enlargement, Combust. Sci. Technol. 24 (1980) 197–210. doi:10.1080/00102208008952438.
[22] S.L. Singer, A.F. Ghoniem, Comprehensive gasification modelling of char particles with multi-modal pore structures, Combust. Flame. 160 (2013) 120–137.
[23] G.F. Froment, K.B. Bischoff, Chemical reactor analysis and design, Wiley, 1990.